Journal of
Mechanics of
Materials and Structures

EXPERIMENTAL AND COMPUTATIONAL EVALUATION OF COMPRESSIVE RESPONSE OF SINGLE AND HEX-ARRAYED ALUMINUM TUBES

Sia Nemat-Nasser, Mahmoud Reza Amini, Jeom Yong Choi
and Jon Isaacs

Volume 2, Nº 10 December 2007

mathematical sciences publishers

JOURNAL OF MECHANICS OF MATERIALS AND STRUCTURES
Vol. 2, No. 10, 2007

EXPERIMENTAL AND COMPUTATIONAL EVALUATION OF COMPRESSIVE RESPONSE OF SINGLE AND HEX-ARRAYED ALUMINUM TUBES

SIA NEMAT-NASSER, MAHMOUD REZA AMINI, JEOM YONG CHOI AND JON ISAACS

We report experiments and simulations of the dynamic and quasistatic compressive response of single and hex-arrayed thick aluminum tubes. The investigation aims to further characterize how tube-based sandwich structures absorb energy. First, we study by compression tests the quasistatic buckling of single tubes of 7075 aluminum, an alloy showing sufficient ductility and plasticity to make it potentially a good choice for energy absorbing devices. The experiments show geometry-dependent buckling modes. The corresponding finite element numerical simulations correlate well and will help estimate the maximum load level, and the buckling and postbuckling responses. Second, we study the dynamic buckling of sandwiched, hex-arrayed 3003 aluminum tubes. The simulations and experimental results correlate well and show a remarkable increase in energy absorbing capacity, which is caused by the postbuckling interaction of neighboring tubes. They also show that, as the tube spacing is decreased, the overall energy absorbed increases significantly. We also simulate how varying tube length and thickness affect the buckling of the array under dynamic loading.

1. Introduction

Metal components absorb energy well because they deform before failing. Plastic deformation, specifically plastic tube buckling, can effectively dissipate large amounts of energy. Circular tubes can absorb more energy with their favorable stroke length per unit mass.

Sandwich structures, consisting of two plates separated by metal tubes, may mitigate impulsive (short duration) loads. Reid [1993] suggested tubes exhibit excellent energy absorbing characteristics when loaded by high velocity impacts. Others have suggested ways to improve the crashworthiness of sandwiches, for example, by varying the tubes' cross sectional geometry. Among all the cross sections examined by Mamalis et al. [2003], thick-walled circular tubes exhibited the most stable crash mode. The experimental investigations—for example, [Lee 1962; Batterman 1965; Horton et al. 1966; Johnson et al. 1977; Nemat-Nasser et al. 2007]—have shown that relatively thick shells (radius to thickness ratio $R/t < 50$) buckle axisymmetrically, whereas this symmetry breaks for thinner shells and they instead buckle in a diamond pattern. Lee [1962], Batterman [1965], and Tennyson and Muggeridege [1969] have found that initial imperfections can significantly influence diamond-shaped circumferential mode buckling (when $R/t < 100$), according to an incremental theory.

In contrast to the elastic response, Gerard [1962] reported in inelastic buckling that the axisymmetric solution always corresponds to a lower buckling stress than the asymmetric solution with circumferential

Keywords: sandwich structures, aluminum tubes, dynamic compression, quasistatic compression, LS_DYNA, physics-based material model.

This work has been supported by ONR (MURI) grant N000140210666 to the University of California, San Diego, with Dr. Roshdy G. Barsoum as program manager.

modes, and that the imperfections are of no significance in either case. Theoretical investigations also suggest that plastic buckling is less sensitive to imperfection than elastic. (See Gellin [1979], who used J_2-deformation theory to model thick shells with sinusoidal axisymmetric imperfections).

Using a J_2 corner theory plasticity model, Tvergaard [1983b] compared the elastic and plastic response in cylindrical shells with initial axisymmetric imperfections and showed that they bifurcate into a nonaxisymmetric shape. For sufficiently thin-walled shells, the bifurcation occurs before the load maximum. In thick-walled shells, the axisymmetric deformations are stable beyond the maximum load, at which the collapse localizes into a single outward buckled mode. His investigations also show that localization delays bifurcation considerably, such that a sufficiently thick-walled shell collapses in an axisymmetric mode. Budiansky and Hutchinson [1966] have shown that tubes collapse at lower loading under dynamic compression than under static loading. In other studies, Karagiozova et al. [2000] studied the inertial effects on axisymmetrically deformed cylindrical shells. Weingarten et al. [1964] have experimentally quantified how the buckling coefficient varies with R/t.

In this paper, we report our experimental and numerical investigations of the dynamic and quasistatic response of thick ($R/t < 20$) hex-arrayed and single aluminum tubes under axial compressive loads. We considered aluminum alloys that have good ductility and plasticity at low temperatures and high strain rates, and that do not fracture [Nemat-Nasser and Guo 2004]. We not address the effects of edge constraint, imperfection, and tube length because they do not significantly influence the plastic buckling and postbuckling of thick cylindrical tubes. This assumption is supported by extensive experimental and numerical investigations over the last 50 years.

We present the results of two series of experiments. One consists of quasistatic experiments of single tubes, and the other involves dynamic impact experiments of hex-arrayed tubes. We used an Instron hydraulic testing machine and a Hopkinson bar apparatus for these experiments, respectively. First, we measured the energy absorbing characteristics of single 7075 aluminum tubes under quasistatic loading. Next, we measured through dynamic impact (compression) tests the dynamic behavior of sandwiched, hex-arrayed 3003 aluminum tubes. We accompanied both of these experiments with finite element simulations. The experiments and simulations show that tight, hexagonally packed sandwiches maintain their load carrying capacity even after the initial buckling, as each tube becomes supported by its neighbors. Finite-element simulations also show the how varying tube length and thickness (with constant outer diameter) affects the structure's ability to absorb energy. We find that as the thickness and length increase, the absorbed energy per unit mass also increases, but stops growing at a maximum level; however, if the two geometrical parameters are disproportionately increased, that energy may drop noticeably.

From these experiments and simulations of the dynamic behavior of sandwich structures with tube cores, we conclude that finite element models properly informed by experimental measurements can reliably predict the overall behavior of complex tube-based sandwich structures. Such models can thus become a powerful tool for designing optimal energy absorbing sandwich structures subject to dynamic and static loads.

2. Experimental procedure and results

Designing crashworthy structures, that is, structures capable of withstanding and mitigating the effect of impact, requires understanding structural dynamics and also the properties and deformation mechanisms

of the material and the larger structure. Axially compressed aluminum tubes absorb energy particularly well, due to their plastic buckling deformation modes. In this section, we report on experiments on the quasistatic compressive behavior of aluminum tubes and pair them with simulations to better understand their deformation mechanisms. All the tubes used in this research are thick-walled with $R/t < 20$. Consequently, we find, the tubes collapse plastically, and the buckling mode and load are insensitive to imperfections and to the length to radius ratio L/R above the proportional limit. As pointed out by Tvergaard [1983b], this can be best explained by axisymmetric localization, which occurs mainly in thick cylindrical shells. We too have observed this localization.

In the following subsection, we describe quasistatic experiments on 7075 aluminum tubes and, in the next subsection, dynamic experiments on the 3003 aluminum hex-arrayed tubes.

2.1. ***Quasistatic experiments and results.*** We performed two quasistatic experiments on two different 7075 aluminum tubes. They are loaded using an Instron hydraulic testing machine with a specially designed arbor. The first tube (tube-I), has $R/t = 18$, while the second (tube-II) has $R/t = 6$. The theory of cylindrical shell buckling considers both tubes to have thick shells, since ($R/t < 100$), and they both buckle plastically.

2.1.1. *Tube I experiment.* Tube I is a 7075 aluminum rod machined into a thick-walled tube of outer diameter 4.50 mm, wall thickness 0.127 mm ($R/t = 18$), and length 11.80 mm. It has a uniform thickness with accurately cut ends. Figure 1 shows a photograph of the arbor consisting of two steel bars (of maraging steel), an aluminum tube specimen, and an extensometer. The specimen is sandwiched between the two bars in the arbor. The experimental setup fixes the tube's ends against lateral displacement but allows them to rotate. The first quasistatic buckling test is conducted at 295 K (room temperature). The load displacement is controlled with a crosshead speed of about 10^{-3} mm/s. An extensomer measures the axial displacement; it is attached to the arbor and calibrated before testing. Signals from the load cell and the extensometer go to a data acquisition system, the SCXI 1001, using Labview software. We analyze these acquired data using suitable calibration factors. Simultaneously, photographs are taken by a digital camera with a close-up lens. The photographs are paired, at each buckling step, with the

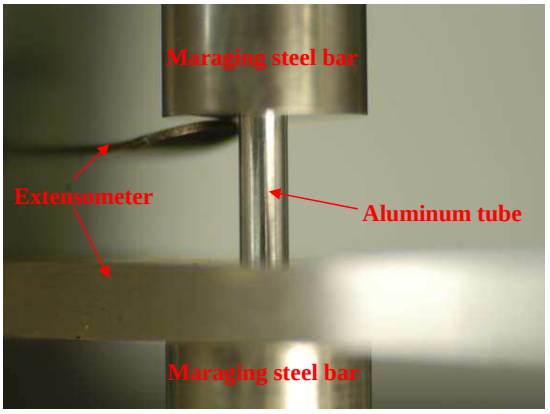

Figure 1. Experimental setup for quasistatic buckling test of 7075 aluminum tube.

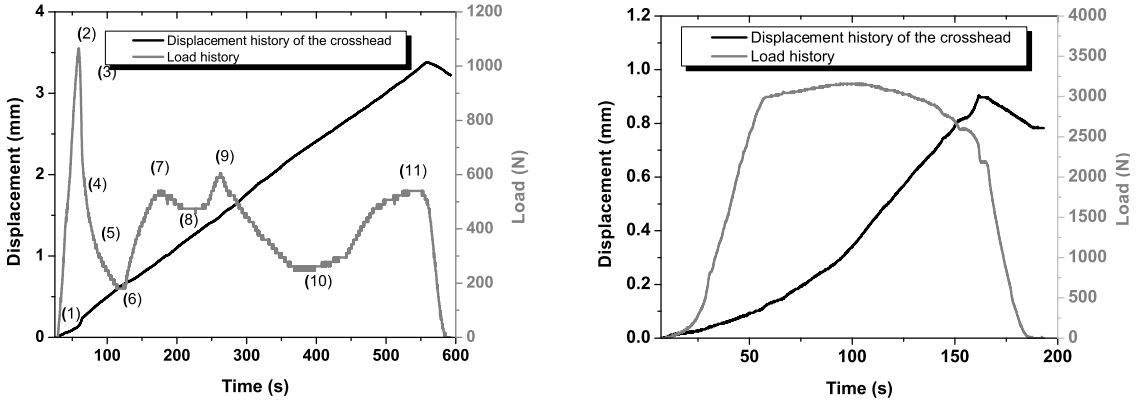

Figure 2. Displacement versus time for aluminum tube-I; displacement-controlled loading with crosshead speed of 6.71×10^{-3} mm/s and corresponding load history. At right, the same for tube-II with crosshead speed 5.33×10^{-2} mm/s.

corresponding load state. Figure 2 (left) displays the load and displacement history for a crosshead speed of 6.71×10^{-3} mm/s.

In the initial stages, the tube deforms in an axisymmetric pattern near one end, as shown in Figure 3. As the axial load is slowly increased, a short axisymmetric bulge develops near one end of the tube (step 1). This bulge continues to grow as the load continues to increase toward a maximum value (step 2); during this time, the load versus displacement curve is linear, indicating elastic deformation. The peak loading corresponds to the first buckling fold. Afterward, the load drops off while the bulge develops into an axisymmetric ring (from step 3 to step 6). The maximum load that the tube can sustain is defined to be the buckling load; the corresponding mode is the buckling mode. This buckling mode is called a ring mode in the literature.

After the initial symmetric or concentric deformation, the tube begins to deform in an asymmetric or diamond (third harmonic) mode at a load less than the bucking load (steps 9 and 11 in Figure 3). We note

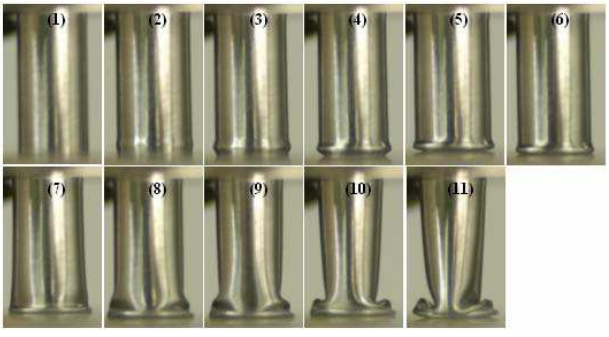

Figure 3. Photographs of aluminum tube-I buckling in uniaxial compression; displacement-controlled loading with crosshead speed 6.71×10^{-3} mm/s: numbers indicate the load state in Figure 2; see [Nemat-Nasser et al. 2006].

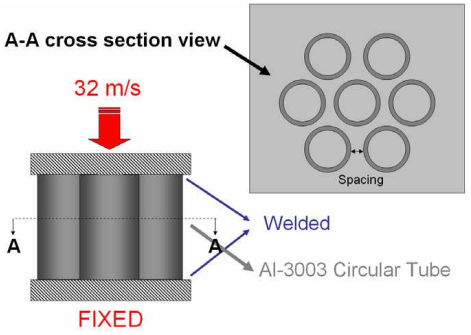

Figure 4. Schematic cross-sectional and lateral views of a hex-arrayed tube structure.

that the static axial crushing tests by Mamalis and Johnson [1983] and Abramowicz and Jones [1984] on aluminum circular cylinders exhibited similar behavior.

2.1.2. *Tube II experiment.* Tube II is a 7075 aluminum rod machined into a thick-walled tube of outer diameter 4.52 mm, wall thickness 0.381 mm ($R/t = 6$), and length 8.76 mm. The experimental setup is exactly the same as in the first experiment. The total displacement in this test is less than 1 mm, and no postbuckling folding is observed. Figure 2 (right) displays how the load and displacement vary with time under displacement-controlled loading with a crosshead speed of 5.33×10^{-2} mm/s.

2.2. ***Dynamic experiments and results.*** The hex-arrayed tube structure consists of two square plates and seven 3003 aluminum tubes, each of outer diameter 15.87 mm, wall thickness 1.65 mm, and height 12.7 mm ($R/t = 5$). Figure 4 shows the cross sectional and lateral views. Each sample is individually fabricated, and hence it may have slight geometric and dimensional imperfections.

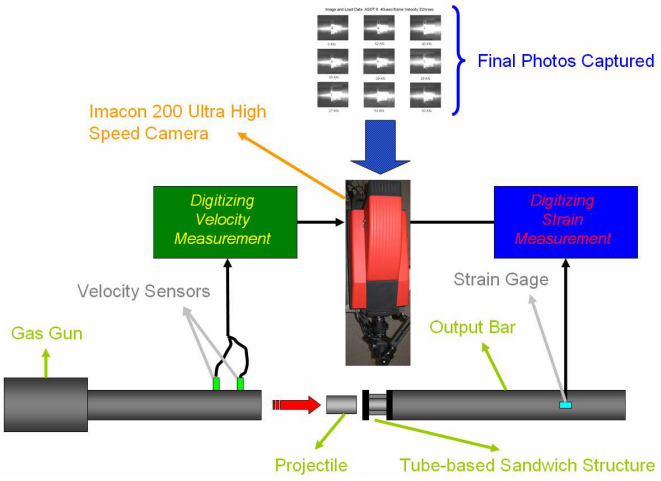

Figure 5. Schematic view of the dynamic compression test of hex-arrayed tubes and Hopkinson bar equipment setup.

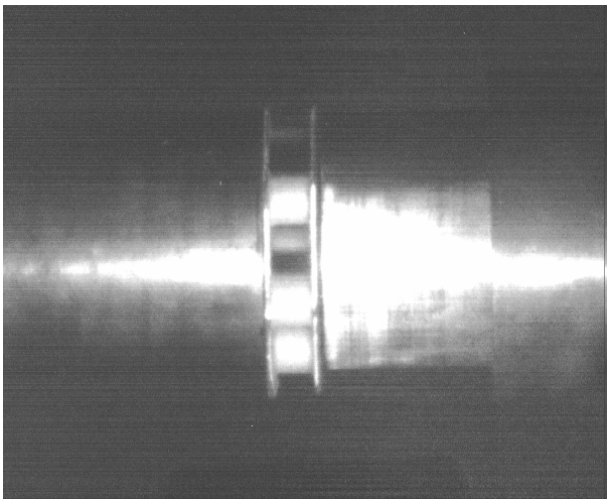

Figure 6. A photo of the hex-arrayed structure attached to the output Hopkinson bar.

The dynamic tests use a single Hopkinson bar setup, shown in Figures 5, 6 and 7. A hex-arrayed sandwich structure is impacted by a striker bar at 32m/s. The deformation process is documented using an Imacon 200 high-speed camera. Just before impact, the striker bar velocity is measured by the sensors near the end of the gas gun. The force transmitted through the structure is measured by a strain gauge attached to the 3 inch output bar. The 7075 aluminum striker bar has a 3 inch (7.62 cm) diameter, length 4.5 inch (11.43 cm), and weight 1460 g. Below, we report our experimental results for three tests, denoted as test-I, test-II, and test-III, corresponding to tube spacings of less than 0.1 inch (2.5 mm), 0.2 inch (5 mm), and 0.5 inch (12.5 mm). Figure 8 shows the top view of two such hex-arrayed structures.

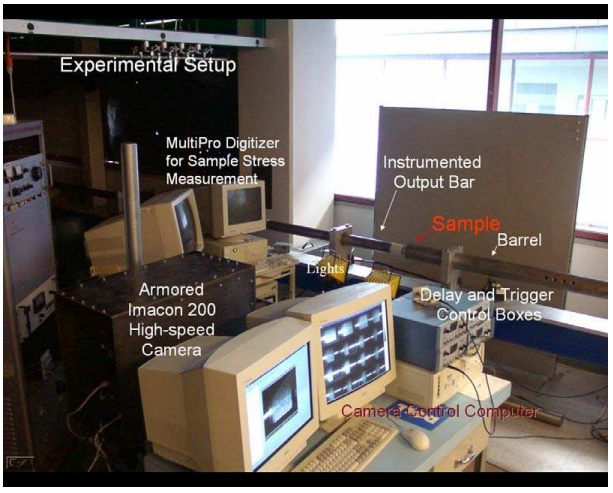

Figure 7. Experimental setup for dynamic compression test of hex-arrayed tubes.

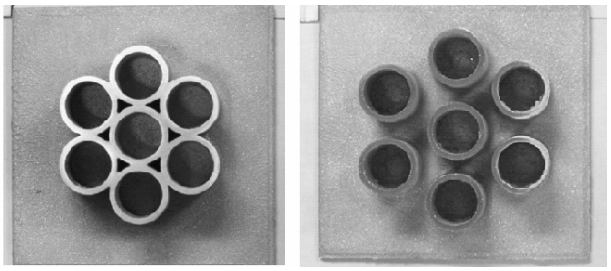

Figure 8. Top view of the hex-arrayed 3003 aluminum tubes. (a) compact spacing (< 0.1 inch), (b) loose spacing ($= 0.5$ inch).

Figure 9 shows the deformed configuration of the test-II specimen captured by the high-speed camera at 40 μs time intervals. In Figure 10 the vertical lines mark the camera timing, and the curve plots the compressive load transmitted through the sandwich structure, as recorded by the strain gauge attached to the output bar.

Figure 11 presents the load versus displacement curves of three tests. The load is normalized by the mass of the corresponding structure to properly compare arrayed tube structures of different length, thickness, and outer diameter. The load versus displacement curves show that the transmitted postbuckling load decreases as the tube spacing is increased. The response of the two structures with greater tube spacing (0.2 inch and 0.5 inch) follows the classic tube buckling pattern: the load drops off after reaching a peak value, although there is slight postbuckling interaction of the 0.2 inch spaced tubes. On the other hand, because adjacent tubes interact in the tightly-packed structure (0.1 inch tube spacing), their postbuckling plastic deformation is interrelated and more complex. A slightly larger buckling load is essentially maintained over the entire deformation process and even increases at large displacements.

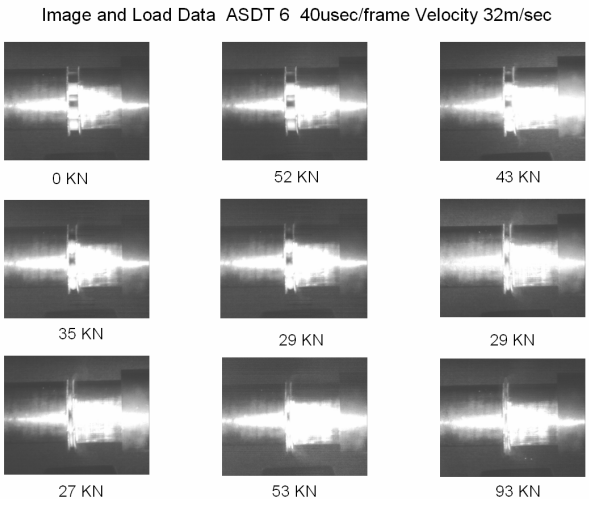

Figure 9. The deformed shape of the test II specimen captured by an Imacon-200 high-speed camera at 40 μs intervals.

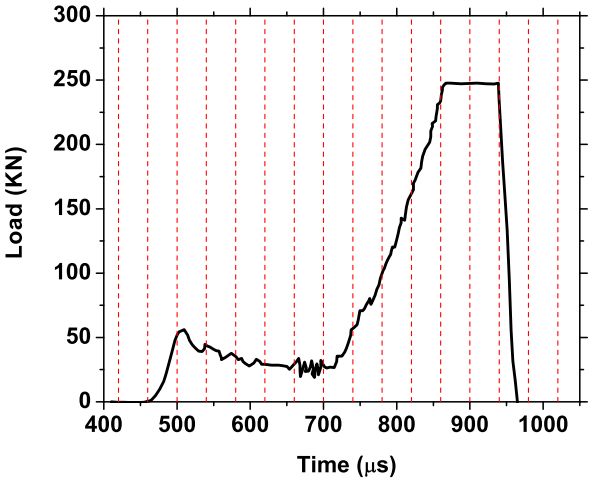

Figure 10. The vertical lines show the camera timing and the curve presents the compressive load history of the structure obtained from the strain gauges attached to the output bar.

3. Material models

We detail the material constitutive models used in this study. For the tubes, we use the Johnson–Cook material model that is already provided by the LS-DYNA, using material parameters that have been experimentally established by Rule and Jones [1998] for 7075 aluminum. In this model the flow stress τ is expressed as

$$\tau = (A + B\gamma^n)(1 + C \ln \dot{\varepsilon}^*)(1 - T^{*m}),$$

where $\dot{\varepsilon}^* = \dot{\gamma}/\dot{\gamma}_0$ is the dimensionless strain rate, ($\dot{\gamma}_0$ is normally taken to be 1.0/s); the parameters A, B and C, are material constants; γ is the effective plastic strain; and T^* is a normalized temperature

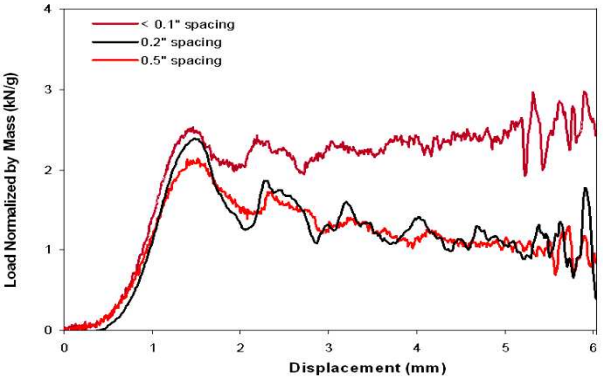

Figure 11. Illustration of normalized load-displacement experimental relations for test-I, test-II and test-III; Load is normalized by the mass of the system. Tube dimensions: OD = 15.87 mm; wall thickness = 1.65 mm; and length = 12.7 mm.

defined by

$$T^* = \frac{T - T_r}{T_m - T_r},$$

where $T_m = 877\,\mathrm{K}$ is the melting temperature of the material. T is the material's actual temperature, and T_r is a reference temperature which must be less than the lowest temperature of interest; we have used $T_r = 298\,\mathrm{K}$. The complete expression for the Johnson–Cook model for 7075 aluminum is (in MPa)

$$\tau = (452 + 457\gamma^{0.357})(1 + 0.01 \ln \dot{\varepsilon}^*)(1 - T^{*1.1}),$$

where,

$$T^* = \frac{T - 298}{579}.$$

To model the 3003 aluminum tubes, we have implemented a user-defined physics-based (PB) material model [Nemat-Nasser and Guo 2004] into LS-DYNA. This is an elastic-viscoplastic constitutive model developed using the kinetics and kinematics of dislocation motion; see [Nemat-Nasser 2004] for details. We evaluate the resulting macroscopic constitutive parameters using a series of quasistatic and dynamic experiments over a broad range of temperatures and strain rates. The model is thus reliable and can be used to simulate high strain-rate deformations, for example, those involved in blast-induced plastic deformations and shear banding. In this model the flow stress τ is expressed as a function of temperature T, effective plastic strain γ, and effective plastic strain rate $\dot{\gamma}$ as

$$\tau = \begin{cases} c_0 + c_1\gamma^n + \tau^0 \left(1 - \left[\frac{-kT}{G_0}\left(\ln\frac{\dot{\gamma}}{\dot{\gamma}_0} + \ln f(\gamma, T)\right)\right]^{\frac{1}{q}}\right)^{\frac{1}{p}} f(\gamma, T), & \text{for } T \le T_c, \\ c_0 + c_1\gamma^{n_1}, & \text{for } T \ge T_c, \end{cases}$$

where

$$f(\gamma, T) = 1 + a\left[1 - \left(\frac{T}{T_m}\right)^2\right]\gamma^m, \qquad T_c = \frac{-G_0}{k}\left(\ln\frac{\dot{\gamma}}{\dot{\gamma}_0} + \ln f(\gamma, T)\right)^{-1}$$

and where G_0 is the total energy of the short-range barrier to the motion of dislocations, measured per atom; k is the Boltzmann constant; $\dot{\gamma}_0$ is a reference strain rate; T_m is the melting temperature; and c_0, c_1, τ^0, n, m, p, q, and a are material parameters. Nemat-Nasser [2004] detail the parameters used in the PB model. The final constitutive relation for this material is

$$\tau = \begin{cases} 64\gamma^{0.4} + 72\left\{1 - \left[-3.2 \times 10^{-5} T\left(\ln\frac{\dot{\gamma}}{2\times 10^{10}} + \ln f(\gamma, T)\right)\right]^{\frac{1}{2}}\right\}^{\frac{3}{2}} f(\gamma, T), & \text{for } T \le T_c, \\ 64\gamma^{0.4}, & \text{for } T \ge T_c, \end{cases}$$

where

$$f(\gamma, T) = 1 + 6\left[1 - \left(\frac{T}{916}\right)^2\right]\gamma^{0.05}, \qquad T_c = \left[-3.2 \times 10^5\left(\ln\frac{\dot{\gamma}}{2\times 10^{10}} + \ln f(\gamma, T)\right)\right]^{-1}$$

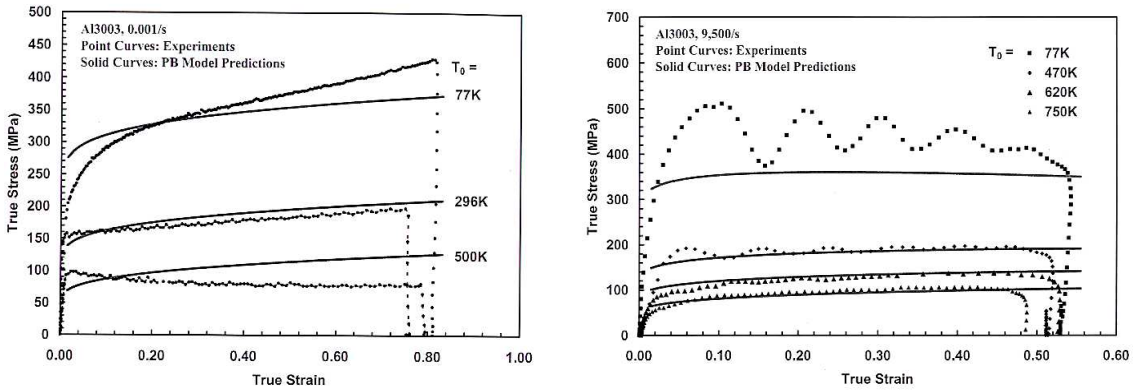

Figure 12. Comparison of PB-model (physical-based model) predictions with experimental results at strain rates of 0.0001 /s and 9500 /s. Initial temperatures obtained by Nemat-Nasser and Guo [2004].

the stress is in MPa, and T is in degrees Kelvin. Figure 12 compares the experimental results with the PB-model predictions at strain rates of 10^{-3} /s and 9500 /s, for indicated initial temperatures. As is seen, the model correlates well with the experimental data.

4. Numerical simulation procedures

We now report the results of our simulations of the nonlinear dynamic and static deformation and buckling of single and hex-arrayed tubes. We used the finite element LS-DYNA 970 code that incorporates experimentally-based nonlinear material models, including strain-rate and temperature effects. The code is based on an updated Lagrangian formulation; it is fully vectorized and can be used to analyze the transient dynamic response of solids and structures [Hallquist 2001].

4.1. ***Finite element model.*** We model hex-arrayed and single tubes using 4-node Belytschko–Tasy shell elements with two Gauss integration points through the thickness and an hourglass viscosity to damp out the zero-energy modes. The mesh density is optimized to capture smoothly and with reasonable computational cost the buckling geometry and structural collapse. The code automatically models the contact between adjacent tubes through its single-surface contact option. We model the sandwich plates as rigid walls and consider the nodes of the tubes as slave nodes. We assume fixed boundary conditions at both ends of all the tubes, because, in our experiments, the tubes are welded to the top and bottom plates of the sandwich structure.

4.2. ***Numerical integration of plasticity model.*** To apply the constitutive models presented in Section 3 for the three-dimensional calculations, the J_2-plasticity model is integrated using a radial return algorithm. In this semiimplicit backward Euler method, increments in the effective plastic strain and temperature are calculating after the time step, and then the flow-stress condition is enforced. Given the total strain tensor ε_n, the plastic strain tensor ε_n^p, the effective plastic strain γ_n, the stress tensor σ_n at time n, and the total strain-increment tensor $\Delta\varepsilon = \dot{\varepsilon}\,\Delta t$, the code computes the quantities $(\varepsilon_{n+1}, \varepsilon_{n+1}^p, \gamma_{n+1}, \sigma_{n+1})$, as follows:

(i) The trial stress $\sigma^{(0)}$ is computed by the elastic predictor using

$$\sigma^{(0)} = \sigma_n + 2G\Delta\varepsilon' + K\,\mathrm{trace}(\Delta\varepsilon),$$

where $\Delta\varepsilon'$ is the deviator of the total strain-increment tensor, G is the shear modulus, and K is the bulk modulus.

(ii) The effective plastic strain rate $\dot{\gamma}_{n+1}$ follows from assuming the strain increment is all plastic. This is a reasonable approximation because the elastic part is negligibly small.

(iii) The effective trial stress $\bar{\sigma}^{(0)}$ is computed and compared with the current flow stress, $\tau(\gamma_n, \dot{\gamma}_{n+1}, T_n)$ (discussed in Section 3). If the trial state is elastic, the effective plastic strain, plastic strain-rate, and temperature are not updated, and the trial stress is used as the stress at the end of the time step. However, if the effective trial stress exceeds the flow stress, then the radial return algorithm for plastic loading is applied in four steps:

(a) Initialization:

$$k = 0, \qquad \varepsilon^{p(0)} = \varepsilon_n^p, \qquad \gamma^{(0)} = \gamma_n, \qquad \Delta\gamma^{(0)} = 0, \tag{4–1}$$

where k is the iteration counter and superscripts correspond to the iteration number.

(b) Check flow stress at the kth iteration:

$$f^{(k)} = \bar{\sigma}^{(k)} - \tau\big(\gamma^{(k)}, \dot{\gamma}_{n+1}, T_n\big). \tag{4–2}$$

If $f^{(k)} < \mathrm{TOL}$ (an arbitrary small number, here 10^{-5}), then the iteration has converged and the temperature is updated; otherwise the process is continued.

(c) Compute the increment in the effective plastic strain:

$$\delta\gamma = \frac{\bar{\sigma}^{(0)} - 3G\Delta\gamma - \tau\big(\gamma^{(k)}, \dot{\gamma}_{n+1}, T_n\big)}{3G + \frac{\partial\tau}{\partial\gamma}\big(\gamma^{(k)}, \dot{\gamma}_{n+1}, T_n\big)}, \qquad \Delta\gamma^{(k+1)} = \Delta\gamma^{(k)} + \delta\gamma. \tag{4–3}$$

(d) Update the plastic strain tensor, effective plastic strain and total stress, set $k \leftarrow k+1$, and go to step (iii.b).

5. Numerical simulation of single-tube buckling

In this section, we present results of the finite element simulation of the quasistatic tube buckling and compare them with the experiments. We compare both the buckling load and mode, and focus on the postbuckling behavior. We discuss some relevant published analytical results.

In general, the finite element simulations agree well with the experimental results, both for the buckling load and the buckling mode. On the other hand, the previously published analytical predictions we have examined do not seem to yield accurate estimates of the buckling load, nor do they predict the observed postbuckling behavior.

5.1. ***Computational results.*** The simulation of tube-I predicts that the tube initially buckles at one end in an axisymmetric mode. As the crushing continues, the buckling mode changes from an axisymmetric bulge to a triangular shape. The mode changes during the postbuckling process because the boundary condition changes for the remaining unbuckled portion of the cylinder. The simulated buckling mode and

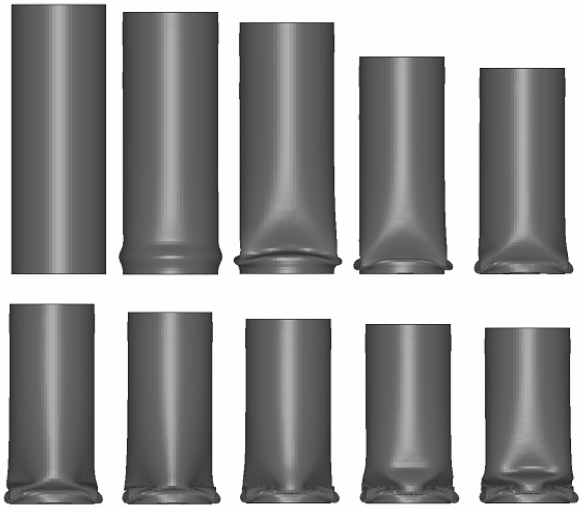

Figure 13. Sequence of plots from deformation and buckling of the 7075 aluminum tube-I in the finite element model with uniaxial compression; displacement-controlled loading with crosshead speed 6.71×10^{-3} mm/s, presented in Figure 2.

its changes during loading agree fairly well with the experimental results; see Figures 13 (left) and 14 (left).

For the simulation, we apply the displacement boundary conditions discussed for the experiments in Figure 2. It predicts the buckling load to be 910 N, whereas the experimental buckling load is 1051 N,

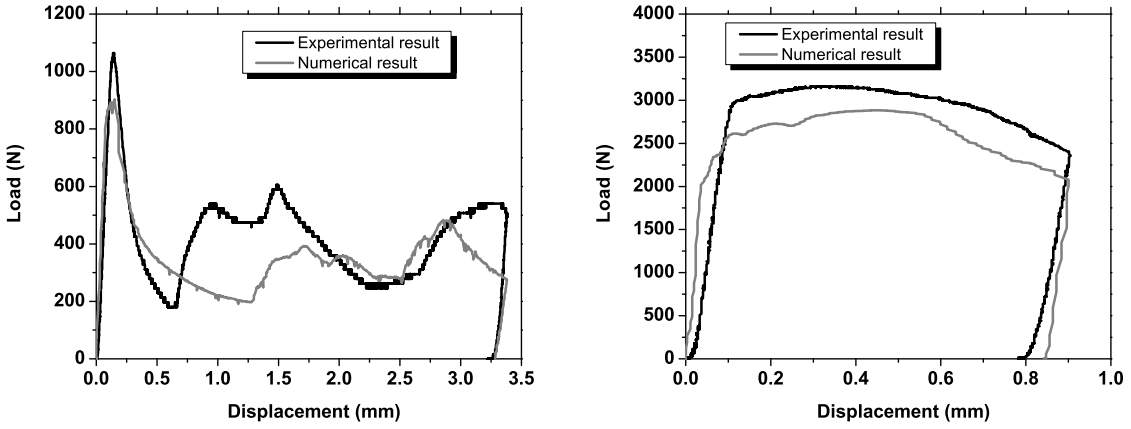

Figure 14. Comparison of experimental and numerical load variation with displacement of the crosshead for 7075 aluminum tube-I, of dimensions: OD = 4.50 mm; wall thickness = 0.127 mm; and length = 11.80 mm. At right, the same for tube-II, of dimensions: OD = 4.52 mm; wall thickness = 0.381 mm; and length = 8.76 mm.

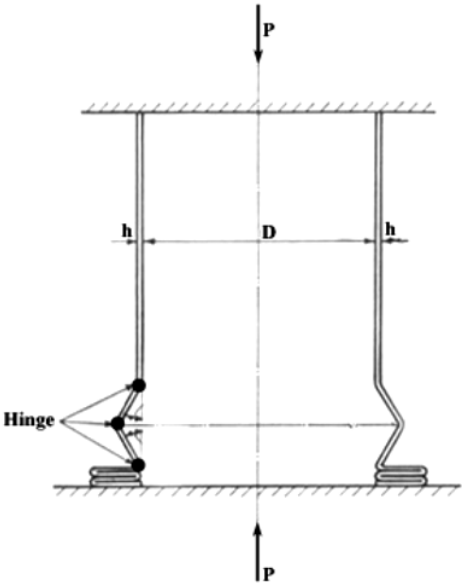

Figure 15. Axisymmetric axial buckling collapse mechanism due to Alexander [1960].

for a 13.4% error. The simulation produces three postbuckling peaks which agree with the experimental results both in number and in their approximate values.

Abramowicz and Jones [1984] have provided a comprehensive review and substantial data on the axisymmetric buckling modes of cylindrical shells. Their analysis is based on work done by Alexander [1960]. Their assumed buckling mechanism, illustrated in Figure 15, takes place in a section of length $2H$ and consists of three stationary (relative to the material) plastic hinges separating two outward moving portions which stretch circumferentially. Abramowicz and Jones determine the crushing force P_B in terms of the material properties and tube geometry after minimizing the global work and arrive at the following expression:

$$\frac{4P_B}{\sigma_0 t^2} = 20.79\left(\frac{D}{t}\right)^{1/2} + 11.90,$$

where σ_0 is the yield stress of the material, t is the thickness, and D is the outer diameter. For our experiment described above, this equation gives $P_B = 225.5\,\text{N}$, whereas, the experimental mean crushing force is approximately 452 N. This significant underestimation typifies predictions of this analysis and is ascribed by Alexander [1960] to the assumption that the convolutions flatten into discs. That assumption is inconsistent with our experimental observations and numerical simulations. Ignoring the plastic hardening is another possible reason for this underestimation.

For aluminum tube-II, shown in Figures 14 (right) and 16 (right), the numerical model provides a reasonable representation of the experimental results, both for the buckling load and the buckling mode. The simulation predicts the buckling load to be around 2600 N, whereas, the experiment shows a buckling load of 2950 N, for an 11.8% error. Figure 14 compares the experimental and numerical load-displacement curves. The simulation predicts that the buckling starts at the end of the tube and also

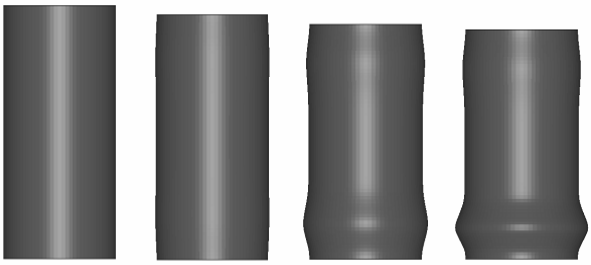

Figure 16. Sequence of plots from simulating deformation and buckling of the thick 7075 aluminum tube in uniaxial compression; displacement-controlled loading with crosshead speed 5.33×10^{-2} mm/s, presented in Figure 2.

when the displacement reaches a specific level; see Figure 16. It predicts a stable postbuckling response that agrees with the experimental observations.

Two important observations about the buckling mode are apparent from the foregoing numerical and experimental results. First, the buckling mode is axisymmetric, and, second, the buckling begins near the ends of the tubes. We explain these observations as follows.

Axisymmetric buckling has only stretching in the hoop direction, whereas nonaxisymmetric buckling primarily involves bending in that direction. The energy required for either mode, that is, hoop direction stretching or hoop direction bending, is a function of tube thickness. As this increases, the energy required for stretching increases linearly. On the other hand, the bending energy varies quadratically with the thickness, making it increase more rapidly with thickness. For sufficiently thick tubes (roughly $R/t < 40$), the hoop bending energy exceeds the hoop membrane energy, and thus the buckling occurs in the lower energy axisymmetric mode [Allan 1968].

That buckling begins at the ends can be explained by the end boundary conditions and axisymmetric buckling localization theory [Tvergaard 1983a]. If the tubes were not constrained at the ends, then, as the load increases, the axial shortening would cause a radial expansion that is uniform along the axis (Poisson effect). However, because the tubes are constrained at both ends by friction, there arises an axisymmetric, radial shear stress which begins at the tube ends and decays rapidly away from the boundary. This additional shear stress triggers localized axisymmetric buckling at the boundaries. This behavior is observed in the quasistatic experiments and predicted by the finite element simulations.

6. Numerical simulation of hex-arrayed tube-buckling

To enhance energy absorption while keeping the system as light as possible, one may exploit the post-buckling interaction of adjacent tubes. As for a single tube, hex-arrayed tubes initially respond linearly to a compressive load. However, after they begin to buckle, they begin to interact with one another, enhancing the energy absorption of the structure.

How hex-arrayed tubes respond to a compressive load depends on their spacing. Here, we present the experimental and numerical results of dynamic compression tests of hex-arrayed tubes and document the effect of varying tube spacing, length, and thickness (for a fixed outer diameter).

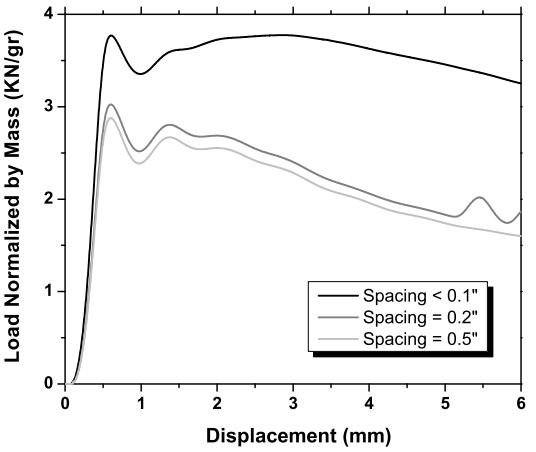

Figure 17. The numerical results of normalized load per mass with displacement variation of the sandwich plates for the hex-arrayed 3003 aluminum tubes compared at three different spacing levels, using Nemat-Nasser's physics-based (PB) material model. Tube dimensions: OD = 15.9 mm; wall thickness = 1.65 mm; and length = 13.0 mm.

6.1. ***Computational results.*** Each tube has outer diameter 15.87 mm, wall thickness 1.65 mm, and height 13.0 mm ($R/t = 5$). All the simulations are performed with the same setup, using an impact speed of 32 m/s. Their fixed boundary conditions simulate welding the tubes to the plates. Figure 17 compares the load histories for the three simulations. For all three tube spacings, they predict a buckling load per unit mass of approximately 3 KN/g, while the experiments show this value to be 2.6 KN/g. Although the numerical models qualitatively predict the experimental trends, the remaining quantitative discrepancy is not fully understood. It may be that the fabrication has introduced various imperfections in the samples [Meissner 2004], while the simulation assumes perfectly arranged hex-array structures.

The finite element model predicts that the tight structure (gaps < 0.1 inch) maintains the load level, perhaps because the tubes interact after buckling. The experiment shows the same effect. For less tight structures, with tube spacings of 0.2 inch and 0.5 inch, the load histories are almost the same, although the 0.2 inch one exhibits some postbuckling interaction. The finite element simulations predict lower buckling loads than for the tight structure, which is in good agreement with the experimental results; see Figure 14. The simulations predict reasonably well how the overall behavior and the energy absorption depend on the tube spacing. Figure 18 presents the predicted final deformed configuration of the tubes with 0.2 inch spacing; Figure 19 shows the corresponding deformation sequences.

Figure 18. Final finite element configuration of the hex-arrayed 3003 aluminum tubes at maximum deformation; spacing equal to 0.2 inch, using Nemat-Nasser's physics-based material model.

Figure 19. Sequence of numerical prediction of hex-arrayed tube structure buckling with 0.2 inch spacing, under dynamic loading.

6.2. ***Parametric study of hex-arrayed tube-buckling.*** We have simulated how the arrays respond to varying thickness and length, while keeping the outer diameter constant at 1.59 cm. To sensibly compare the results, we normalize the dissipated energy and the applied load by the mass of the system. All

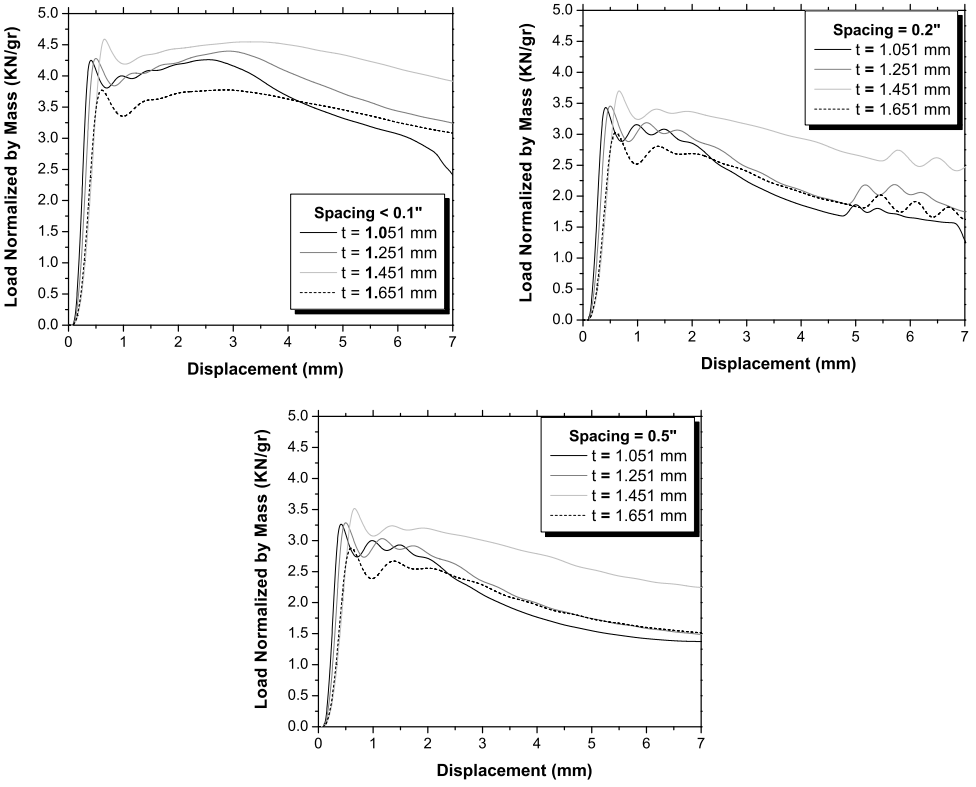

Figure 20. Effect of thickness on the normalized load per unit mass variation with displacement of the sandwich plates. The tubes have spacing less than 0.1 inch, equal to .02 inch, and equal to .05 inch. They have lengths 1.3 cm and outer diameter 1.59 cm.

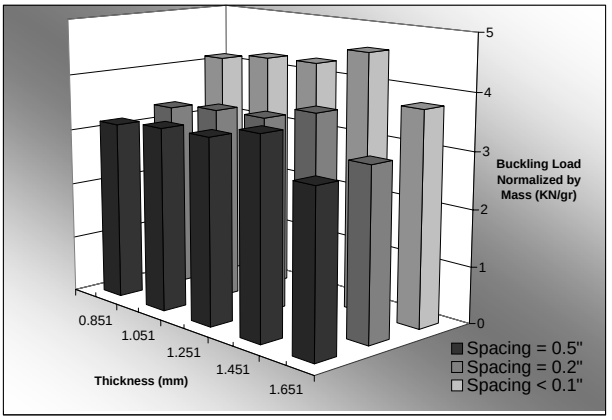

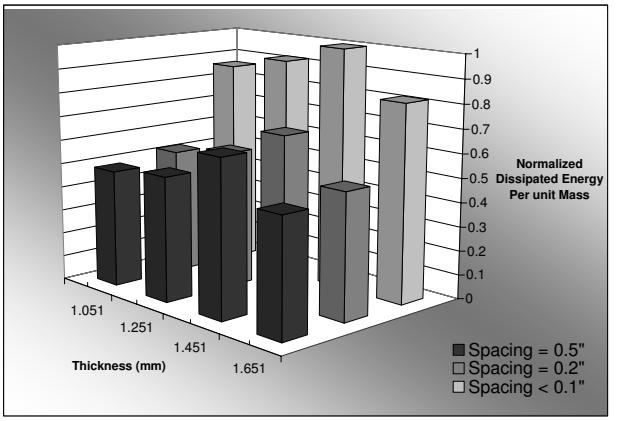

Figure 21. Buckling load and dissipated energy per unit mass of the hex-arrayed tube structure, normalized and plotted against varying thickness and spacing levels. The length of the tubes is 1.3 cm and the outer diameter is 1.59 cm.

simulations have the same fixed boundary conditions, with a 32 m/s impact velocity. We model aluminum 3003 using Nemat-Nasser's PB model, presented in Section 2.

To analyze the effect varying tube thickness, we chose five different values of 0.851, 1.051, 1.251, 1.451, and 1.651 mm, while keeping the length at 1.30 cm and the outer diameter at 1.59 cm. For each thickness, we studied all three tube spacings considered in the previous section. Figure 20 shows the simulation results. Increasing the thickness from 1.051 to 1.451 mm causes an increase in the normalized load for all three tube spacings. However, further increasing the thickness from 1.451 to 1.651 mm does

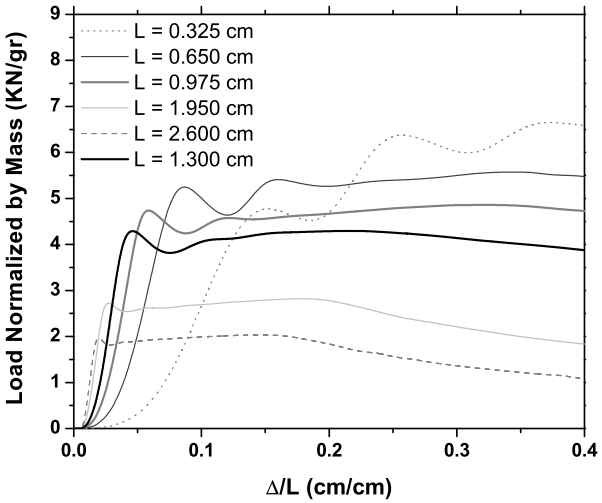

Figure 22. Variation of normalized load per unit mass of the hex-arrayed tube structure with deflection of unit length for tubes of different lengths and compact spacing ($<$ 0.1 inch). The outer diameter of the 3003 aluminum tubes is 1.59 cm.

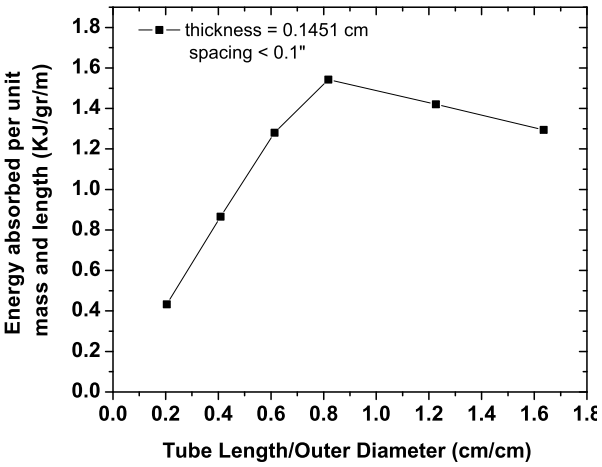

Figure 23. Variation of energy absorbed per unit mass and length of the hex-arrayed aluminum tube structure with different length to outer diameter ratios. The spacing is compact (< 0.1 inch) and the thickness is 0.145 cm.

not cause a significant drop in the normalized buckling load or the normalized dissipated energy. For comparison, we further rescale the normalized dissipated energies by the largest one, namely, that of the tightly spaced tubes with thickness 1.451 mm; see Figure 21.

To analyze the effect of varying tube length, we choose various lengths L from 0.32 cm to 2.60 cm, while keeping a fixed outer diameter at 1.59 cm, the thickness at 1.451 mm, and a spacing less than 0.1 inch. The simulations show that, as L/R increases, the buckling mode changes from a single barrel in the middle to a double barrel at the ends. This change occurred as L went from 1.3 cm to 1.95 cm. Figure 22 illustrates how the rescaled, normalized load varies with the deflection per unit length of the tubes. As length increases, starting from 0.325 cm, the absorbed energy (per unit mass per unit length) increases and reaches a maximum at 1.3 cm; however, increasing the length further does not seem to result in an increase in the absorbed energy (per unit mass, per unit length), as is illustrated in Figure 23. Among the simulations conducted in this study, the hex-arrayed tube structure with an outer diameter to thickness $\mathrm{OD}/t = 11$ and outer diameter to length $\mathrm{OD}/L = 1.22$ showed the best energy-absorption performance.

7. Conclusions

We measured and simulated quasistatic buckling of single aluminum tubes and dynamic buckling of hex-arrayed aluminum tubes. The methods achieved excellent agreement in the buckling load, buckling mode, and the postbuckling behavior. The finite element calculations incorporate rate- and temperature-sensitive physics-based constitutive models for aluminum 3003 that we integrated into LS-DYNA using a J_2-plasticity model and a radial-return algorithm.

The single tube experiments and simulations have confirmed that the buckling mode—that is, the deformation path of least resistance—depends on the geometrical ratios and the tube thickness. The

single tube initially buckled into an axisymmetric pattern near one end, and then, as the load level significantly dropped, continued into a diamond deformation mode.

The experiments and simulation of the hex-arrayed tube structures suggest that their energy absorption increases with a decrease in their spacing, due to postbuckling interaction between the adjacent tubes. Finally, we examined how varying the array's geometrical parameters affected their energy absorption.

References

[Abramowicz and Jones 1984] W. Abramowicz and N. Jones, "Dynamic axial crushing of circular tubes", *Int. J. Impact Eng.* **2**:3 (1984), 263–281.

[Alexander 1960] J. M. Alexander, "An approximate analysis of the collapse of thin cylindrical shells under axial loading", *Quart. J. Mech. Appl. Math.* **13** (1960), 10–15.

[Allan 1968] T. Allan, "Experimental and analytical investigation of the behavior of cylindrical tubes subject to axial compressive forces", *J. Mech. Eng. Sci.* **2** (1968), 182–197.

[Batterman 1965] S. C. Batterman, "Plastic buckling of axially compressed cylindrical shells", *AIAA J.* **3** (1965), 316–325.

[Budiansky and Hutchinson 1966] B. Budiansky and J. W. Hutchinson, "A Survey of some buckling problems", *AIAA J.* **4** (1966), 1505–1510.

[Gellin 1979] S. Gellin, "Effect of an axisymmetric imperfection on the plastic buckling of an axially compressed cylindrical shell", *J. Appl. Mech.* **46** (1979), 125–131.

[Gerard 1962] G. Gerard, "On the role of initial imperfections in plastic buckling of cylinders under axial compression", *J. Aerosp. Sci. Technol.* **29** (1962), 744–745.

[Hallquist 2001] J. O. Hallquist, *LS-DYNA Version 970: Theoretical manual*, Livermore: Livermore Software Technology Corporation, 2001.

[Horton et al. 1966] W. H. Horton, S. C. Bailey, and A. M. Edwards, "Nonsymmetric buckle patterns in progressive plastic buckling", *Exp. Mech.* **23** (1966), 433–444.

[Johnson et al. 1977] W. Johnson, P. D. Soden, and S. T. S. Al-Hassani, "Inextensional collapse of thin walled tubes under axial compression", *J. Strain Anal. Eng. Des.* **12** (1977), 317–330.

[Karagiozova et al. 2000] D. Karagiozova, M. Alves, and N. Jones, "Inertia effects in axisymmetrically deformed cylindrical shells under axial impact", *Int. J. Impact Eng.* **24** (2000), 1083–1115.

[Lee 1962] L. H. N. Lee, "Inelastic buckling of initially imperfect cylinder shells subject to axial compression", *J. Aerosp. Sci. Technol.* **29** (1962), 87–95.

[Mamalis and Johnson 1983] A. G. Mamalis and W. Johnson, "The quasi-static crumpling of thin-walled circular cylinders and frusta under axial compression", *Int. J. Mech. Sci.* **25** (1983), 713–732.

[Mamalis et al. 2003] A. G. Mamalis, D. E. Manolakos, M. B. Ioannidis, P. K. Kostazos, and C. Dimitriou, "Finite element simulation of the axial collapse of metallic thin-walled tubes with octagonal cross-section", *Thin-Walled Struct.* **41** (2003), 891–900.

[Meissner 2004] J. Meissner, "Axially aligned cylindrical shell arrays as energy absorbing structures", Master's Thesis, UC San Diego, August 2004.

[Nemat-Nasser 2004] S. Nemat-Nasser, *Plasticity a treatise on finite deformation of heterogeneous inelastic materials*, first ed., Cambridge University press, Cambridge, 2004.

[Nemat-Nasser and Guo 2004] S. Nemat-Nasser and W. G. Guo, "Plastic flow of Al 3003 alloy over a wide range of strain rates and temperatures: experimental and modeling", 2004. unpublished work.

[Nemat-Nasser et al. 2006] S. Nemat-Nasser, J. Choi, J. B. Isaacs, and D. W. Lischer, "Quasistatic and dynamic buckling of thin cylindrical shape memory shells", *J. Appl. Mech.* **73** (2006), 825–833. Special Volume on Current Trends in Mechanics, W.G. Khauss 2004 Symposium.

[Nemat-Nasser et al. 2007] S. Nemat-Nasser, W. J. Kang, J. D. McGee, W. G. Guo, and J. B. Issacs, "Experimental investigation of energy-absorption characteristics of sandwich structures", *Int. J. Impact Eng.* **34**:6 (2007), 1119–1146.

[Reid 1993] S. R. Reid, "Plastic deformation mechanisms in axially compressed metal tubes used as impact energy absorbers", *Int. J. Mech. Sci.* **12** (1993), 1035–1052.

[Rule and Jones 1998] W. K. Rule and S. E. Jones, "A revised form for the Johnson-Cook strength model", *Int. J. Impact Eng.* **21**:8 (1998), 609–624.

[Tennyson and Muggeridege 1969] R. C. Tennyson and D. B. Muggeridege, "Buckling of axisymmetric imperfect circular cylinder shells under axial compression", *AIAA J.* **7** (1969), 2127–2131.

[Tvergaard 1983a] V. Tvergaard, "On the transition from diamond mode to an axisymmetric mode of collapse in cylindrical shells", *Int. J. Solids Struct.* **19**:10 (1983), 845–856.

[Tvergaard 1983b] V. Tvergaard, "Plastic buckling of axially compressed circular cylindrical shells", *Thin-Walled Struct.* **1** (1983), 139–163.

[Weingarten et al. 1964] V. I. Weingarten, E. J. Morgan, and P. Seide, "Elastic stability of thin-walled cylindrical and conical shells under axial compression", *AIAA J.* **3** (1964), 500–505.

Received 20 May 2007. Accepted 23 May 2007.

SIA NEMAT-NASSER: sia@ucsd.edu
Center of Excellence for Advanced Materials, Department of Mechanical and Aerospace Engineering, University of California San Diego, La Jolla, CA 92093-0416, United States

MAHMOUD REZA AMINI: mramini@starlite.ucsd.edu
Center of Excellence for Advanced Materials, Department of Mechanical and Aerospace Engineering, University of California San Diego, La Jolla, CA 92093-0416, United States

JEOM YONG CHOI: jjeomyong@posco.co.kr
POSCO Technical Research Laboratories, Pohang, Kyeongbuk, 790–785, Korea

JON ISAACS: JonIsaacs@aol.com
Center of Excellence for Advanced Materials, Department of Mechanical and Aerospace Engineering, University of California San Diego, La Jolla, CA 92093-0416, United States